Environmental Pollution 400 (2026) 128234

Contents lists available at ScienceDirect

Environmental Pollution

journal homepage: www.elsevier.com/locate/envpol

Source-oriented probabilistic ecological and human health risk assessment of urban road dust using an open-source framework in a tropical coastal city

Tra Van Tung [a], Tinh H.T. Nguyen [b], Tanapon Phenrat [c,d], Tran Cong-Thanh [e,f], Ly Sy Phu Nguyen [e,f], Vinh Son Lam [g], Bui Pham Phuong Thanh [h], Nguyen Xuan Cuong [b,i], Quoc Ba Tran [b,i,*]

[a] Faculty of Applied Science and Technology, Nguyen Tat Thanh University, Ho Chi Minh City, Viet Nam
[b] Faculty of Environmental and Chemical Engineering, Duy Tan University, Danang, Viet Nam
[c] Research Unit for Integrated Natural Resources Remediation and Reclamation (IN3R), Department of Civil Engineering, Faculty of Engineering, Naresuan University, Phitsanulok, Thailand
[d] AI-CARE Research Cluster, Naresuan University, Phitsanulok, 65000, Thailand
[e] Vietnam National University, Ho Chi Minh City, Viet Nam
[f] Faculty of Environment, University of Science, Ho Chi Minh City, Viet Nam
[g] HUTECH Institute of Applied Sciences, HUTECH University, Ho Chi Minh City, Viet Nam
[h] Department of Resource and Environmental Management, Thu Dau Mot University, Ho Chi Minh City, Viet Nam
[i] Institute of Research and Development, Duy Tan University, Danang, Viet Nam

ARTICLE INFO

Keywords:
Urban road dust
Potentially toxic elements
PMF source apportionment
Monte Carlo simulation
Probabilistic risk assessment

ABSTRACT

Urban road dust (URD) acts as both a sink and a secondary emission source of potentially toxic elements (PTEs), posing ecological and human health risks in rapidly urbanizing cities. Although source-oriented probabilistic risk assessment integrating positive matrix factorization (PMF) with Monte Carlo simulation (MCS) has advanced, applications remain largely confined to industrial cities and often rely on commercial software, limiting reproducibility and transferability. Here, we develop and apply a fully open-source PMF-MCS framework implemented in R to quantify pollution characteristics, source contributions, and probabilistic ecological and human health risks of nine PTEs in URD from Da Nang, a tropical coastal city in central Vietnam. Three dominant sources were identified based on PMF inference: traffic (44.8%), service-industrial activities (30.1%), and natural background (25.2%). Cd (1.28 mg/kg) and Sb (1.62 mg/kg) exhibited strong enrichment, with Sb controlling 71-94% of the integrated pollution index ($INI = 3.11$). Mean ecological risk was classified as “low ecological risk” ($NCRI = 102.5$), whereas upper-percentile values (P95 = 351.5) reached “high” to “very high ecological risk”, reflecting localized hotspot conditions rather than widespread city-scale risk, driven by Cd and Sb enriched areas associated with traffic and service-industrial sources. Non-carcinogenic risks remained below thresholds across all populations, while carcinogenic risk fell within the cautionary range (10^{-6}-10^{-4}), particularly for children (mean $TCR = 5.51 \times 10^{-6}$), dominated by As (69-82%) and traffic-related sources (46-48%). This study provides a source-oriented probabilistic assessment of URD in a tropical coastal Southeast Asian city and delivers a transparent, reproducible framework for risk-informed urban environmental management.

1. Introduction

Urban road dust (URD) is an increasing environmental concern under rapid urbanization and industrialization, acting as both a sink and a secondary emission source of potentially toxic elements (PTEs) (Panqing et al., 2023; Ustaoğlu et al., 2026; Zafra-Mejía and Rondón-Quintana, 2025). Accumulated PTEs can be redistributed to the atmosphere, soils, and surface waters through resuspension and runoff, leading to ecological degradation and human health risks (Akindele et al., 2024; Albuja et al., 2024). Common URD-associated PTEs,

* Corresponding author. Institute of Research and Development, Duy Tan University, Danang, Viet Nam.
E-mail address: tranbaquoc@duytan.edu.vn (Q.B. Tran).

https://doi.org/10.1016/j.envpol.2026.128234
Received 4 March 2026; Received in revised form 8 April 2026; Accepted 28 April 2026
Available online 6 May 2026
0269-7491/

including Cd, Sb, As, Pb, Cr, Zn, and Mn, are toxic, persistent, and capable of bioaccumulation, with documented links to neurological, respiratory, cardiovascular, and metabolic disorders. Human exposure occurs primarily through ingestion, inhalation, and dermal contact, with children being particularly vulnerable due to behavioral and physiological factors, as well as increased sensitivity to toxic metals such as lead (Pb), which exerts pronounced neurodevelopmental toxicity in children and fetuses, and arsenic (As), a well-established human carcinogen (Rehman et al., 2025; Yuksel et al., 2017; Yüksel et al., 2010; Zupančič et al., 2024). In tropical coastal cities, dense traffic, mixed industrial and service activities, construction, tourism, and monsoon-driven meteorology further enhance PTE accumulation and resuspension, amplifying environmental and public health risks (Chen et al., 2024; Tran et al., 2025).

Most existing studies on URD contamination, source apportionment, and associated risks have focused on industrial cities in China, Europe, Asia, and parts of North America (Asgari et al., 2025; Chen et al., 2024; Khan et al., 2025; Öncü et al., 2025; Yang et al., 2024). Contamination levels and associated ecological and human health risks are commonly evaluated using deterministic indices such as the geo-accumulation index, enrichment factor, pollution load index, and ecological and health risk index (Adewumi, 2022; Dytłow and Górka-Kostrubiec, 2021). To resolve emission sources, positive matrix factorization (PMF) has been widely applied and, more recently, coupled with Monte Carlo simulation (MCS) to enable source-oriented probabilistic ecological and human health risk assessment, representing a major advance over deterministic approaches (Wang et al., 2023b; Wu et al., 2024; Yang et al., 2024).

Despite these advances, two critical gaps remain. First, PMF-MCS based source-oriented probabilistic risk assessment (SO-PRA) has been applied predominantly in industrial and inland urban settings, especially China, with limited evidence from tropical coastal cities in Southeast Asia, where monsoon-driven resuspension, mixed traffic-tourism-industrial emissions, and rapid urban expansion may alter risk patterns (Asgari et al., 2025; Chen et al., 2024; Wang et al., 2024). Second, existing PMF-MCS studies largely rely on commercial software platforms (e.g., Oracle Crystal Ball), which limit transparency, reproducibility, flexibility in uncertainty analysis, and licensing costs (Öncü et al., 2025; Panqing et al., 2023; Yang et al., 2024). A fully open-source, end-to-end implementation of SO-PRA for URD remains limited.

Against this background, this study investigates URD in Da Nang, a rapidly urbanizing tropical coastal city in central Vietnam. It uses an integrated, fully open-source framework for SO-PRA of PTEs. The study addresses the critical lack of open-source, transferable risk assessment tools for data-limited coastal cities in Southeast Asia, where unique environmental and socio-economic factors may influence risk patterns. The objectives are to: (i) implement MCS fully in the open-source R platform with publicly available scripts; (ii) strengthen PMF-based source apportionment using complementary statistical analyses (Spearman correlation, hierarchical cluster analysis) and GIS spatial coherence to ensure robust source identification; and (iii) quantify source-oriented, probabilistic ecological and human health risks to identify priority emission sources and dominant risk drivers. This study provides a PMF-MCS application in a tropical coastal Southeast Asian city and delivers a transferable open-source framework that supports risk-informed URD management in regions with limited data and technical capacity.

2. Materials and methods

2.1. Study area and road dust sampling

2.1.1. Study area

Da Nang is a rapidly urbanizing tropical coastal city in central Vietnam (15°55′-16°4′ N, 107°18′-108^{0}20′ E), situated on a narrow coastal plain influenced by monsoon circulation. Seasonal contrasts between dry and rainy periods promote the accumulation of urban road dust and its remobilization through resuspension and runoff, enhancing the mobility of particle-bound potentially toxic elements (PTEs) (Tran et al., 2025; Tran, 2025).

Rapid urban expansion has been accompanied by heavy traffic, with approximately 950,000 registered vehicles in 2023, of which more than 90% were motorcycles. Industrial and construction activities contribute 25.3% of the gross regional domestic product and are concentrated in major industrial zones, including Hoa Khanh, Lien Chieu, Hoa Cam, and the Da Nang High-Tech Park, while tourism and services remain key economic drivers (Tran, 2025). This combination of dense traffic, mixed industrial activities, and coastal monsoon conditions makes Da Nang representative for examining source-oriented probabilistic risks of PTEs in urban road dust in tropical coastal cities of Southeast Asia.

2.1.2. Road dust sampling

A total of 56 urban URD samples were collected in August 2024 from roads representing 56 wards/communes across Da Nang (Fig. 1, black dots). Sampling was conducted under dry conditions, with no rainfall for at least 7 days prior to collection, to minimize wash-off effects. Sampling sites were pre-surveyed and georeferenced using a handheld GPS.

At each site, dust was collected from road shoulders using clean plastic tools after coarse debris was removed. Individual samples (0.75-1.50 kg) were placed in labeled polyethylene bags and transported to the laboratory on the same day for storage under dry conditions prior to processing (Fig. S1). Four background samples, collected from areas minimally affected by traffic and urban activities, were adopted from Tran et al. (2025) to represent local geochemical background levels.

2.2. Chemical analysis and quality control

In the laboratory, URD samples were air-dried and sieved to <100 μm to obtain the fine fraction relevant to resuspension and human exposure (Jeong and Ra, 2022; Osorio-Martinez et al., 2021). Approximately 0.50 g of each sample was digested by microwave-assisted acid digestion (HNO_3-HCl, 2:1), filtered through a 0.45 μm membrane, and analyzed for PTE concentrations using inductively coupled plasma mass spectrometry (ICP-MS; Agilent 7700x). Nine PTEs were quantified: Cd, Sb, As, Pb, Cr, Zn, Mn, Al, and Fe. Quality assurance and quality control included reagent blanks, duplicate samples (n = 10), matrix spikes (n = 5), and certified reference material SRM 1648a (Urban Particulate Matter) (NIST, 2020). Blank values were negligible, duplicate variability was <10%, and recoveries (CRM) ranged from 80 to 110% for all PTEs, indicating satisfactory analytical accuracy and precision. Detailed analytical quality control parameters, including MDLs, method-level limits of detection (LODs), estimated limits of quantification (LOQs), CRM recoveries, and duplicate precision, are summarized in Table S1 (Supporting Information).

2.3. Source apportionment

Source apportionment of PTEs in URD was conducted using the PMF model (v5.0) (US.EPA, 2014) based on measured concentration and uncertainty matrices. The optimal number of factors was determined using Q values, scaled residuals, factor interpretability, and rotational ambiguity. Model robustness was evaluated using diagnostic tools and further supported by Spearman correlation and hierarchical cluster analysis. Detailed PMF configuration and validation are provided in Text S1 and Fig. S2.

2.4. Pollution level assessment

Pollution levels of PTEs in URD were quantified using the geo-accumulation index (*Igeo*) (Müller, 1969):

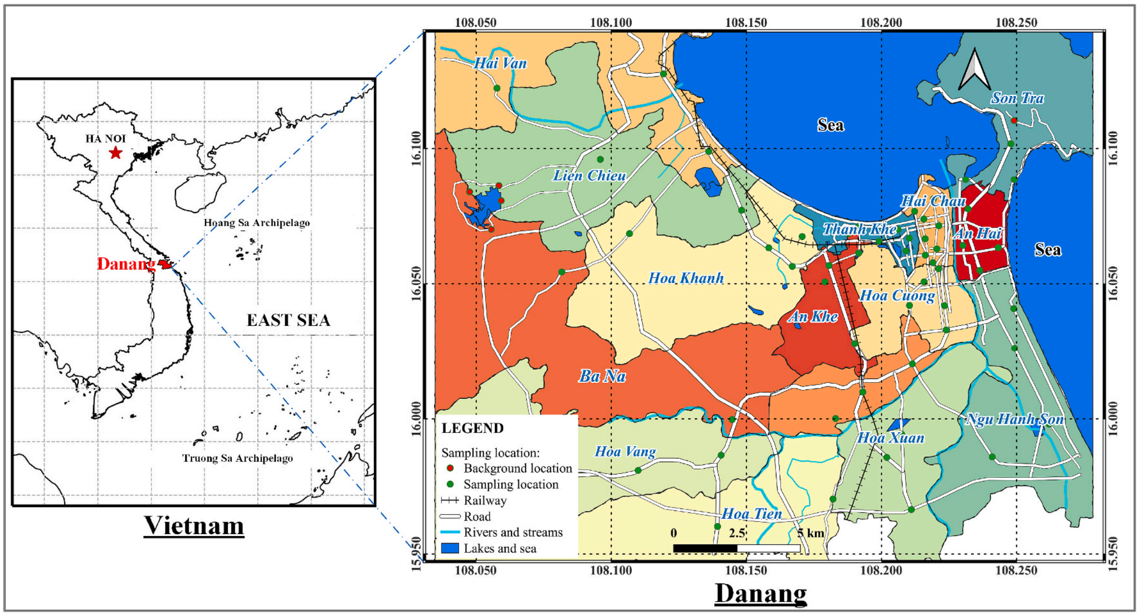

Fig. 1. Study area and URD sampling locations in Da Nang City, Vietnam (sampling sites: green dots; background sites: red dots).

$$I_{geo,i,j} = \log_2\left(\frac{C_{i,j}}{kB_j}\right) \quad (1)$$

where $C_{i,j}$ is the concentration of the element j in sample i, B_j is the local geochemical background value, and k = 1.5 accounts for natural variability.

Integrated pollution intensity was evaluated using the improved Nemerow pollution index (*INI*) (Huang et al., 2021):

$$INI_i = \sqrt{\frac{I^2_{geo(avg),i} + I^2_{geo(\max),i}}{2}} \quad (2)$$

where $I^2_{geo(avg),i}$ and $I^2_{geo(max),i}$ denote the mean and maximum *Igeo* values across elements in sample *i*. Pollution categories are listed in Table S2. Uncertainty was quantified using MCS (Section 2.7).

2.5. Ecological risk assessment

Ecological risks associated with PTEs in URD were evaluated using the potential ecological risk framework by Hakanson (1980), which integrates contamination levels with element-specific toxicity.

2.5.1. Potential ecological risk factor of individual elements

The potential ecological risk factor ($E_{i,j}$) for element *j* in sample *i* was calculated as:

$$E_{i,j} = T_j \times \frac{C_{i,j}}{B_j} \quad (3)$$

where T_j is the toxicity-response factor. Toxicity factors were adopted from the literature: Cd = 30, As = 10, Pb = 5, Cr = 2, Zn = 1 (Hakanson, 1980), (Sb = 7) (Wang et al., 2018), and Mn = 1 (Luo et al., 2020).

2.5.2. Integrated ecological risk index

The integrated ecological risk was expressed using the Nemerow composite ecological risk index (*NCRI*):

$$NCRI_i = \sqrt{\frac{E^2_{i,avg} + E^2_{i,\max}}{2}} \quad (4)$$

where $E_{i,avg}$ and $E_{i,max}$ are the mean and maximum $E_{i,j}$ values across all elements. Risk categories are provided in Table S2.

2.5.3. Source-oriented probabilistic ecological risk assessment

Source-oriented ecological risk was assessed by integrating PMF outputs. Source-resolved concentrations of the element j in sample i attributable to the source k were estimated as:

$$C^k_{i,j} = C_{i,k} \times F_{k,j} \quad (5)$$

These concentrations were used to calculate $E_{i,j}$ and *NCRI* for individual sources. Uncertainty was propagated using MCS (Section 2.7), and results are presented as probability distributions. The analytical workflow is shown in Fig. S3.

2.6. Health risk assessment

Human health risks from PTE exposure in URD were assessed for children, adult females, and adult males across ingestion, inhalation, and dermal contact pathways.

2.6.1. Exposure dose estimation

Average daily dose (ADD) of element j in sample i was estimated as:

$$\text{Ingestion}: \quad ADD_{ing,i,j} = \frac{C_{i,j} \times R_{Ing} \times EF \times ED}{BW \times AT} \times 10^{-6} \quad (6)$$

$$\text{Inhalation}: \quad ADD_{inh,i,j} = \frac{C_{i,j} \times R_{Inh} \times EF \times ED}{PEF \times BW \times AT} \quad (7)$$

$$\text{Dermal contact}: \quad ADD_{der,i,j} = \frac{C_{i,j} \times SA \times AF \times ABF \times EF \times ED}{BW \times AT} \times 10^{-6} \quad (8)$$

PTE concentrations were derived from chemical analysis, and exposure parameters were adopted from the literature (Table S3).

2.6.2. Non-carcinogenic risk assessment

Non-carcinogenic risk was expressed as the hazard quotient (*HQ*):

$$HQ_{path,i,j} = \frac{ADD_{path,i,j}}{RfD_{path,j}} \quad (9)$$

where $HQ_{path,i,j}$ is the hazard quotient of the element j via pathway path, and $RfD_{path,j}$ is the pathway-specific reference dose (Table S4).

The hazard index (*HI*) was calculated as:

$$HI_i = \sum_j \sum_{path} HQ_{path,i,j} \quad (10)$$

Potential health concern is indicated when $HI > 1$.

2.6.3. Carcinogenic risk assessment

Carcinogenic risk for carcinogenic elements (Cd, As, Pb, and Cr) was calculated as:

$$CR_{path,i,j} = ADD_{path,i,j} \times SF_{path,j} \quad (11)$$

where $CR_{path,i,j}$ is the carcinogenic risk and $SF_{path,j}$ is the pathway-specific slope factor (Table S4).

Total carcinogenic risk (*TCR*) was calculated as:

$$TCR_i = \sum_j \sum_{path} CR_{path,i,j} \quad (12)$$

$TCR < 10^{-6}$ is considered "acceptable", $10^{-6} < TCR < 10^{-4}$ indicates "potential carcinogenic risk", whereas $TCR > 10^{-4}$ is considered "unacceptable" (US.EPA, 2009).

2.6.4. Source-oriented probabilistic human health risk assessment

Source-oriented probabilistic health risks were quantified by combining PMF-resolved sources with MCS to specifically estimate *HI* and *TCR* for each source. This approach enables the identification of how individual source categories contribute to overall health risks. Source-resolved PTE concentrations provided the basis for calculating exposure and corresponding health risk indices. MCS was used to propagate uncertainty, and *HI* and *TCR* outcomes are presented as distributions with key percentiles (P5, P50, P95) to directly assess the likelihood of risk exceedance. The process is depicted in Fig. S3.

2.7. Uncertainty and sensitivity analysis

Uncertainty in pollution indices and ecological and health risks was quantified through 10,000-iteration MCS in R (v4.4.2). By modeling PTE concentrations with lognormal distributions and using variable-specific distributions for exposure parameters (see Table S3), the analysis highlights which PTEs, pathways, and source inputs most strongly influence risk uncertainty. All calculations used open-source R packages, and the analysis workflow can be reproduced using the openly available R scripts (see R Script - SI).

3. Results and discussion

3.1. General characteristics and spatial distribution of PTEs

3.1.1. General statistical characteristics of PTEs

Descriptive statistics of PTE concentrations in URD are summarized in Table 1. Fe and Al dominated the elemental composition, reflecting natural mineral inputs, followed by Zn, Mn, and Cr, while Pb, As, Sb, and Cd occurred at lower mean concentrations. Several elements exhibited wide concentration ranges, particularly Zn, Cr, and Al, indicating substantial spatial heterogeneity. Variability patterns further highlight this contrast, with Cd (71.5%), Cr (52.2%), and Zn (43.2%) showing high variability, whereas Mn (16.7%) and Fe (12.2%) exhibit relatively low variability. Right-skewed distributions and elevated kurtosis for Cd, Sb, As, Cr, and Zn suggest that overall variability is driven by localized enrichment rather than uniformly elevated concentration (Table 1).

Relative to local geochemical background values, Sb showed the strongest enrichment (28-fold), followed by Cd (11.6-fold), Zn (4.5-fold), Cr (3.1-fold), As (2.5-fold), and Pb (1.85-fold). In contrast, Fe (1.22-fold), Mn (1.00-fold), and Al (0.91-fold) were near background levels, supporting their predominant association with natural mineral inputs (Huang et al., 2021; Navrotsky, 1994). High variability and enrichment in Sb, Cd, and Zn indicate a stronger influence from localized anthropogenic sources. Most PTE concentrations in Da Nang are lower than those in heavily industrialized cities (Table S5), but Zn levels are comparatively elevated for this tropical coastal setting. These findings highlight the significance of investigating contamination sources and spatial variation in PTEs to inform targeted risk assessment and remediation strategies, as moderate mean contamination can mask significant local enrichment and heterogeneity.

3.1.2. Spatial distribution of PTEs

Spatial distributions of nine PTEs in URD across Da Nang are shown in Fig. S4, using inverse distance weighting interpolation for 56 sites. Enriched elements (Cd, Sb, Zn, Cr, As, and Pb) exhibited spatial heterogeneity, with high concentrations along major traffic corridors and in industrial zones. In contrast, background-associated elements (Fe, Al, Mn) showed more uniform spatial patterns.

Among enriched PTEs, Cd and Sb formed high-concentration belts along busy roads, whereas Zn and Cr formed localized hotspots in urbanized and industrial areas. Higher peri-urban concentrations correspond to construction and land disturbance, while Pb was more broadly distributed, associated with the primary road network. These contrasts highlight how anthropogenic activities drive localized PTE hotspots and geogenic components remain more uniform, underscoring the importance of spatial heterogeneity for risk evaluation in this tropical coastal city.

The observed patterns align with findings from other Asian cities (Hao et al., 2023; Wang et al., 2024; Wang et al., 2023a), and provide rare evidence by examining a rapidly urbanizing tropical coastal city in Southeast Asia. This study demonstrates that identifying concentration hotspots is crucial for PMF-based source apportionment and SO-PRA, thereby enhancing our understanding of how spatial heterogeneity, rather than uniform background enrichment, drives elevated PTE concentrations and their impact on ecological and human health risks.

3.2. Source identification and quantification

The PMF identified an optimal three-factor solution ($F_{peak} = -0.3$), supported by minimized Q values, 100% model convergence, and robust

Table 1
Descriptive statistics of PTE concentrations (mg/kg) in urban road dust.

Statistic	Cd	Sb	As	Pb	Cr	Mn	Zn	Al	Fe
Mean	1.28	1.62	9.91	28.3	81.3	253	465	10491	22098
SD	0.918	0.619	2.12	8.52	42.4	42.1	201	5120	2697
Min	0.131	0.426	6.24	6.84	16.8	124	65.3	49.9	15702
Max	3.80	2.74	14.5	42.4	171	340	902	19320	26529
CV (%)	71.5	38.1	21.4	30.1	52.2	16.7	43.2	48.8	12.2
Kurtosis	3.39	1.92	2.04	2.23	1.86	3.92	2.31	3.16	2.45
Skewness	1.12	0.015	0.320	−0.492	0.383	−0.510	0.064	−1.02	−0.578
Background value[1]	0.111	0.057	4.01	15.32	26.25	252	103	11549	18164

Note: Mean, arithmetic mean; SD, standard deviation; Min-Max, minimum-maximum; CV (%), coefficient of variation; Kurtosis and Skewness describe distribution shape; Background values represent local soil reference concentrations from Tran et al. (2025).

bootstrap and displacement diagnostics (Tables S6–S8). Bootstrap resampling (n = 100) confirmed stable factor profiles across all three factors, with inter-run profile correlations exceeding 0.95, indicating that source-resolved concentration estimates ($C_{i,j,k}$) used in the source-oriented risk assessment are reliable within model uncertainty. All PTEs were classified as strong variables, with signal-to-noise ratios ≥4.98 (US.EPA, 2014). Observed and PMF-predicted concentrations showed strong agreement (r^2 = 0.88-0.95 for most elements), except for As (r^2 = 0.52), indicating overall satisfactory model performance (Fig. S5).

The PMF analysis resolved three factors contributing 44.8% (Factor 1), 30.1% (Factor 2), and 25.1% (Factor 3) to total PTE concentrations in URD (Fig. 2a). These factors represent inferred source profiles derived from receptor modeling and supported by Spearman correlation analysis ($\rho > 0.6$, $p < 0.05$) and hierarchical clustering, which group elements with similar sources (Fig. 2c–d).

Factor 1 represents the largest contribution (44.8%) and is dominated by traffic-related tracers, including Sb, Zn, Pb, Cd, and Cr. These elements exhibit strong intercorrelations and are spatially associated with major traffic corridors and the urban core (Fig. S4). Based on established source signatures (Table S9), Sb is commonly associated with brake wear, Zn with tire wear and asphalt additives, and Pb, Cd, and Cr are commonly associated with brake abrasion, lubricants, and vehicle-related emissions. The consistency among chemical profiles, spatial patterns, and statistical relationships suggests that Factor 1 represents traffic-related emissions, consistent with previous URD studies (Cao et al., 2021; Gunawardana et al., 2012; Hao et al., 2023; Liu et al., 2020; Mielke et al., 2011; Yang et al., 2023a).

Factor 2 accounts for 30.1% of total PTE concentrations and is mainly characterized by Cd, Cr, and Zn. These elements show strong correlations and are spatially elevated in central service areas and near industrial zones in the city's northwestern part (Fig. S4). According to compiled source information (Table S9), Cd and Cr are commonly associated with fossil fuel combustion, metal processing, and high-temperature industrial activities. There may be some overlap with traffic emissions. Given Da Nang's mixed land-use structure, this factor is interpreted as being associated with mixed service-industrial activities, based on PMF inference and supporting evidence. This interpretation agrees with findings from other rapidly developing urban environments (Dobaradaran et al., 2017; Hao et al., 2023; Krupnova et al., 2020; Kurmus and Mohajerani, 2020; Luo et al., 2022).

Factor 3 accounts for 25.1% of the total PTE burden and is dominated by Al, Fe, and Mn, which form a distinct cluster separated from anthropogenic elements (Fig. 2d). These elements exhibit relatively uniform spatial distributions and low enrichment relative to background levels (Fig. S4; Table 1). This pattern suggests predominant influence from natural mineral inputs. According to the source summary (Table S9), Al and Fe are characteristic of natural mineral dust and

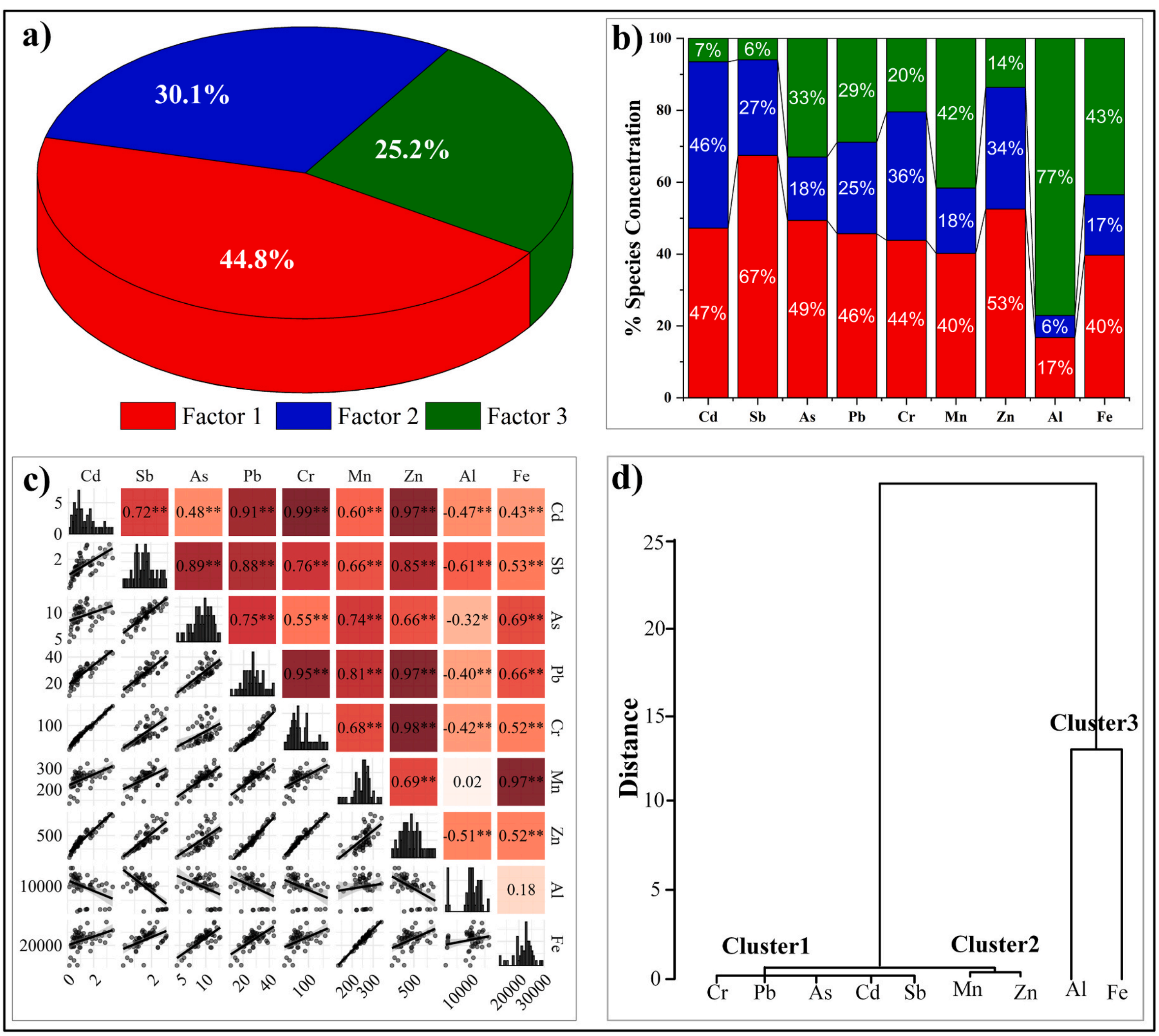

Fig. 2. PMF-based source apportionment of PTEs in urban road dust from Da Nang City: (a) factor contributions; (b) factor chemical profiles; (c) Spearman correlations among PTEs; (d) hierarchical clustering.

crustal materials. Mn is largely associated with weathering processes but may receive secondary anthropogenic inputs at certain urban and industrial sites (Hao et al., 2023; Wang et al., 2024). Accordingly, Factor 3 is interpreted as a natural background source with potential minor anthropogenic influence on Mn.

Overall, the convergence among PMF results, cross-validation, and spatial patterns indicates three dominant source categories: traffic, mixed service-industrial, and natural background, governing PTE concentrations and associated risk in Da Nang. The three-factor PMF solution shows that anthropogenic sources (traffic and service-industrial) dominate total PTE contributions (~75%), despite generally low absolute contamination levels indicated by I_{geo}. This pattern reflects that PMF apportion sources based on relative contributions to observed concentrations rather than absolute enrichment. Notably, this anthropogenic dominance is primarily driven by Cd, Sb, and Zn, which exhibit the highest enrichment ratios (11.6-fold, 28.4-fold, and 4.5-fold above background), whereas elements near background levels contribute smaller mass fractions. Similar patterns reported in previous URD studies (Hao et al., 2023; Wang et al., 2024) confirm the complementary nature of PMF and I_{geo} rather than any inconsistency between the two

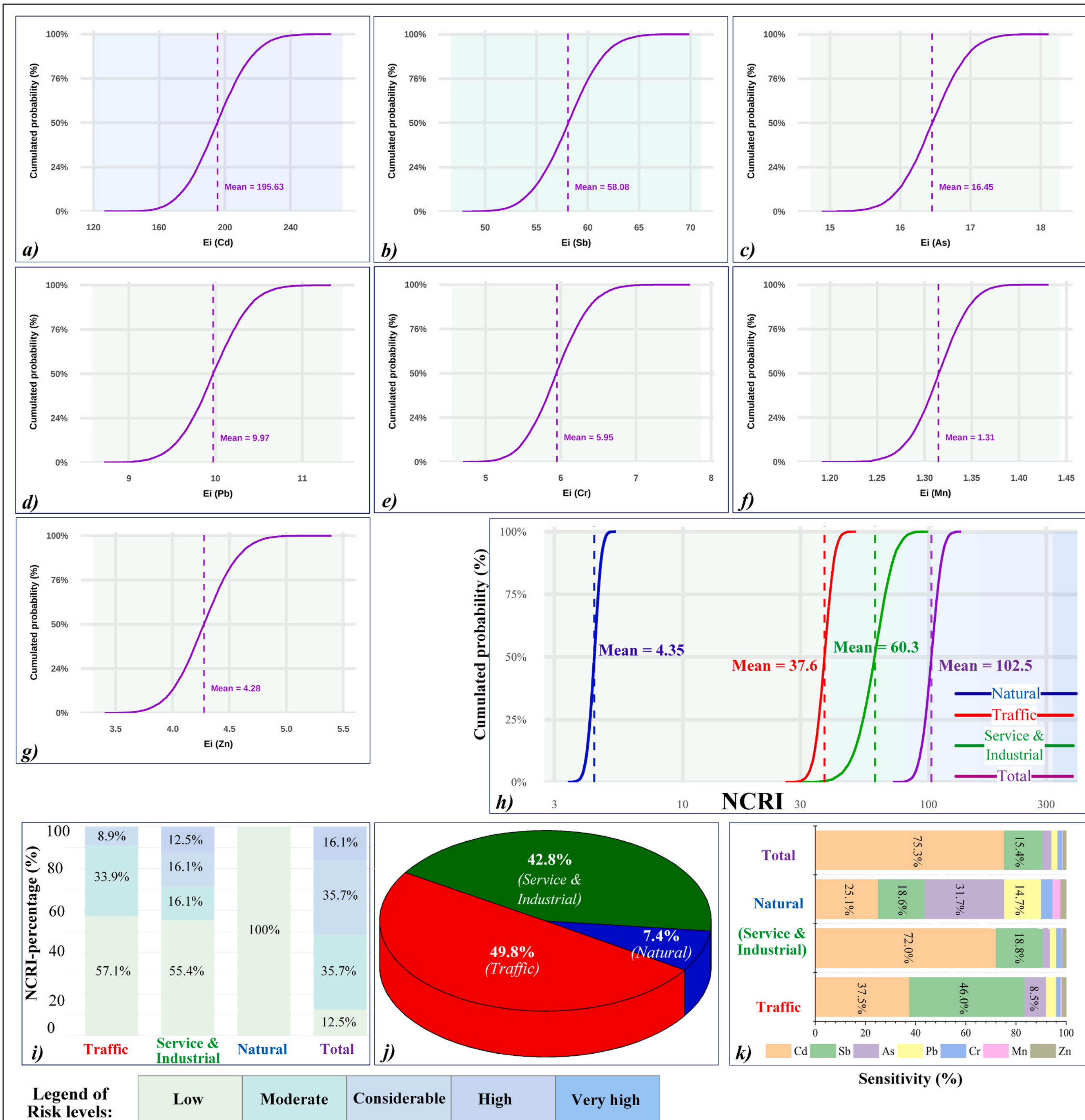

Fig. 3. Probabilistic ecological risk of PTEs in urban road dust based on MCS: (a-g) cumulative distributions of E_i for individual PTEs; (h) cumulative distributions of *NCRI* by source and total; (i) probabilities of ecological risk levels; (j) source contributions to *NCRI*; (k) sensitivity of *NCRI* to individual PTEs.

approaches.

It should be noted that PMF provides inferred source profiles based on statistical decomposition of observed concentrations. Therefore, source identification in this study is interpreted as indicative rather than definitive and is supported by multiple lines of evidence, including correlation analysis, hierarchical clustering, and spatial distribution patterns.

3.3. Probabilistic pollution levels of PTEs

MCSs show strong agreement between simulated and observed mean values for I_{geo} and *INI*, confirming the reliability of the probabilistic framework (Fig. S6). Specifically, detected and simulated means were almost identical for all PTEs: Cd (2.58 vs. 2.59), Sb (4.11 vs. 4.12), As (0.688 vs. 0.687), Pb (0.217 vs. 0.233), Cr (0.826 vs. 0.872), Mn (−0.606 vs. −0.601), Zn (1.41 vs. 1.41), and *INI* (3.07 vs. 3.11), indicating negligible model bias.

Probability distributions reveal a clear pattern in which a subset of elements (notably Cd, Sb, Cr, and Zn) dominates pollution levels, with most probabilities falling within $I_{geo} > 1$, corresponding to moderate to high contamination. In contrast, other elements (e.g., As, Pb and Mn) are generally associated with lower pollution categories, indicating limited overall contribution to contamination (Fig. S6; Table S10).

P5-P95 ranges further highlight this contrast, with wider intervals observed for enriched elements, especially Cd (0.804-4.40), Sb (3.04-5.14), and Zn (0.088-2.77), reflecting spatial heterogeneity and episodic sources (Table S10). At the integrated level, *INI* probabilities are mainly in the range $2 \leq INI < 3$ (40.6%) and $3 \leq INI < 4$ (56.6%), indicating moderate-to-high pollution overall. Sensitivity analysis supports this pattern, showing that *INI* variability is primarily controlled by Sb (70.9-93.7%), followed by Cd (1.8-5.4%), with other PTEs contributing less than 1% (Fig. S6k). Overall, these results indicate that pollution intensity in URD is governed by a small subset of enriched and spatially variable elements, forming the basis for subsequent source-oriented ecological and health risk assessments.

3.4. Ecological risk

3.4.1. Content-oriented ecological risk assessment

MCS results for Ei and *NCRI* are presented in Fig. 3a–h and Table S12. Simulated means closely match detected estimates for all PTEs: Cd (195.6 vs 205.0), Sb (58.1 vs 58.7), As (16.5 vs 17.3), Pb (10.0 vs 10.2), Cr (6.0 vs 6.5), Mn (1.3 vs 1.3), Zn (4.3 vs 4.6), and *NCRI* (102.5 vs 108.4). Together, these results confirm the robustness of the probabilistic framework.

Ecological risk is strongly dominated by a limited subset of elements, with Cd contributing the largest (mean Ei = 195.6; P95 = 488.7), followed by Sb (mean Ei = 58.1). By contrast, other PTEs (As, Pb, Cr, Zn, and Mn) fall into the low-risk category, indicating that overall ecological risk is controlled by a few enriched elements rather than evenly distributed across all PTEs (Fig. 3a–g).

At the integrated level, the mean *NCRI* value (102.5) indicates low overall ecological risk at the city scale. In contrast, the P95 reaches 351.5, corresponding to a high-to-very-high risk level at upper percentiles (Fig. 3h). This contrast reflects spatial heterogeneity, where elevated risk is confined to the upper tail of the probabilistic distribution and represents localized hotspot probabilities rather than widespread city-scale risk. Therefore, reliance on mean values alone may underestimate site-specific ecological threats in heterogeneous urban environments.

3.4.2. Source-oriented ecological risk assessment

Source-oriented results further highlight consistent patterns in ecological distribution (Fig. 3h–k). At the mean level, the service-industrial source has the highest mean *NCRI* (60.3), followed by traffic (37.6), while the natural source contributes minimally (4.35). In terms of probabilities, high (16.1%) and very high (12.5%) risks mainly originate from service-industrial sources. In contrast, traffic risks are mostly low to moderate, and natural sources consistently contribute low risks (Fig. 3i). The source-risk linkage is supported by spatial correspondence between high-NCRI sites and emission locations, with traffic and industrial zones aligning with their respective source contributions (Fig. S4).

In terms of total contributions, ecological risk is primarily driven by traffic (49.8%), followed by service-industrial activities (42.8%) and natural sources (7.4%) (Fig. 3j). Sensitivity analysis shows Cd drives total ecological risk (73.3%), followed by Sb (15.4%) and As (7.9%) (Fig. 3k). At the source level, traffic-related risk is driven by Sb (46.0%) and Cd (37.5%), while service-industrial risk is mainly caused by Cd (72.0%) and Sb (18.8%). These results link risk hotspots to service-industrial emissions and highlight Cd as the main ecological risk driver in both assessment approaches.

3.5. Probabilistic health risk assessment of PTEs

3.5.1. Concentration-oriented probabilistic health risk assessment

MCS results show a consistent pattern in which *HI* decreases across population groups in the order: children > adult females > adult males, with respective mean values of 2.27×10^{-1}, 5.27×10^{-2}, and 4.65×10^{-2} (Fig. 4h; Table S13). All P95 values (5.39×10^{-1} for children, 1.35×10^{-1} for adult females, 1.20×10^{-1} for adult males) remain below the $HI = 1$ benchmark, indicating acceptable non-carcinogenic risk for all groups. However, right-skewed ECDFs, particularly among children, suggest that upper-tail exposures may occur in specific subpopulations and are not fully captured by mean values (Fig. 4h).

Non-carcinogenic risk is primarily driven by a limited group of elements, with Cr and As contributing most across all population groups. For instance, in children, $HQ_{Cr} = 1.02 \times 10^{-1}$ and $HQ_{As} = 7.69 \times 10^{-2}$. Pb and Sb show lower contributions, while Mn, Zn, and Cd have only marginal effects (Fig. 4a–g; Table S13). This consistent pattern indicates that risk is controlled by dominant toxic elements rather than evenly distributed across all PTEs.

For carcinogenic risk, a similar pattern is observed, with mean *TCR* values consistently higher in children (mean: 5.51×10^{-6}, P95: 1.26×10^{-5}) than adult females (mean: 4.25×10^{-6}, P95: 9.85×10^{-6}), and adult males (mean: 3.80×10^{-6}, P95: 8.81×10^{-6}) (Fig. 5e; Table S13). All *TCR* distributions fall within the US. EPA-recommended cautionary range (10^{-6}-10^{-4}). Carcinogenic risk is overwhelmingly dominated by As (69-82% of total TCR), whereas Cd and Cr play secondary roles and other elements remain negligible (Fig. 5a–c,d; Table S13).

Sensitivity analysis (Fig. S7) further highlights that variability in health risk is primarily controlled by exposure - related parameters (exposure duration, exposure frequency, dust ingestion rate, and body weight), whereas dermal-contact parameters have a minor influence. Overall, concentration-based probabilistic results indicate that non-carcinogenic risks from URD in Da Nang remain within acceptable limits. In contrast, carcinogenic risks are driven by upper-tail conditions associated with As exposure, fall within the conventional cautionary range (10^{-6}-10^{-4}), particularly in children. This pattern underscores the importance of considering both population vulnerability and probabilistic variability when assessing health risks in rapidly urbanizing tropical coastal cities.

3.5.2. Source-oriented probabilistic health risk assessment

Source-oriented probabilistic health risks were quantified by integrating PMF-resolved sources with MCS. This approach enabled the attribution of non-carcinogenic and carcinogenic risks to specific sources: traffic, service-industrial, and natural, for children, adult females, and adult males (Fig. 6). The source-risk linkage is supported by PMF bootstrap stability (Tables S6–S8) and spatial correspondence with emission locations (Fig. S4), confirming the reliability of PMF-resolved inputs.

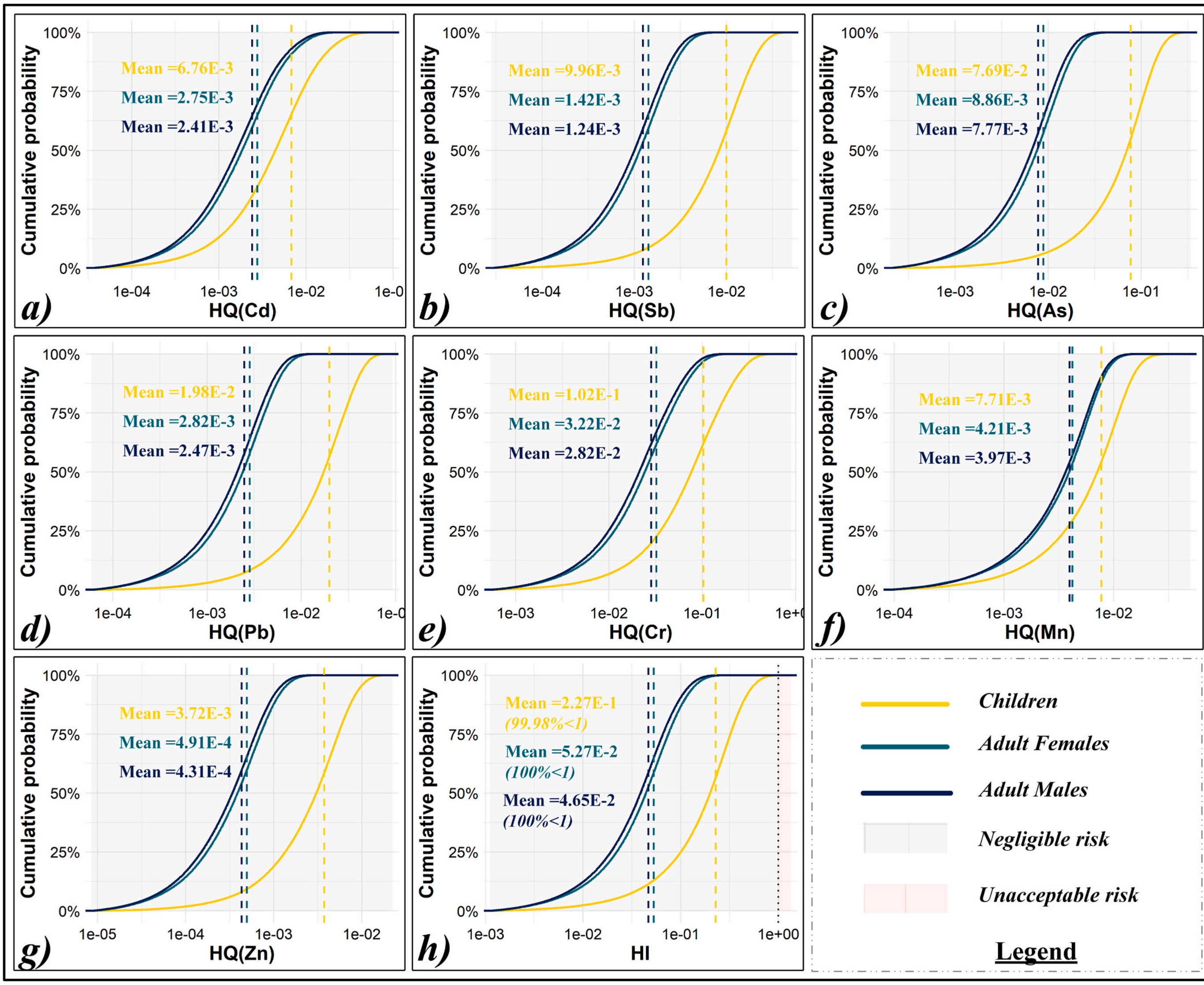

Fig. 4. ECDFs of non-carcinogenic risk: (a-g) *HQ* for each PTE, (h) total *HI* for children, adult females, and adult males. Dashed lines show means; dotted lines show the benchmark (*HQ* or *HI* = 1).

Across all sources and population groups, mean *HI* values remain well below the non-carcinogenic threshold ($HI = 1$), indicating low overall risk. A consistent pattern is observed in which traffic sources contribute the largest share of HI, followed by service-industrial and natural sources. In children, this pattern is most pronounced (mean $HI = 9.37 \times 10^{-2}$ for traffic, 7.32×10^{-2} for service-industrial, and 4.50×10^{-2} for natural sources), with similar but lower magnitudes observed for adults (Fig. 6a1; Table S14). Upper-tail values follow the same trend, with the highest P95 also attributable to traffic sources (2.65×10^{-1}). Source contribution analysis further confirms this pattern, with traffic sources account for 45-46% of total *HI*, service-industrial sources contribute 28-31%, and natural sources composed 24-25% (Fig. 6c1). Exceedance probabilities remain negligible, with ≥99.98% of *HI* values fall below the safety threshold and only marginal exceedance (<0.1%) observed for children (Table S17).

A similar source-dependent pattern is evident for carcinogenic risk. Mean *TCR* values for all sources and population groups were mostly within the cautionary range (10^{-6}-10^{-4}), with higher values consistently observed in children than in adults. In children, mean *TCR* values were highest for traffic (2.36×10^{-6}), followed by service-industrial (1.64×10^{-6}) and natural sources (1.17×10^{-6}). Traffic also dominated the upper tail ($P95 = 6.71 \times 10^{-6}$; Fig. 6b1; Table S14). Patterns for adult females and adult males were similar, though absolute *TCR* values decreased with age (Fig. 6b2-b3; Tables S14–S16). Traffic-related emissions made up about 46-48% of total *TCR*. Service-industrial contributed 25-32%, and natural sources contributed 23-26% (Fig. 6c2). Exceedance analysis showed a high probability of $TCR \geq 10^{-6}$ (84.5-88.9%), especially among children. There were no cases exceeding the unacceptable threshold ($TCR \geq 10^{-4}$) (Table S17).

Overall, these results indicate that health risks are governed by consistent source-related patterns rather than isolated extreme values. Non-carcinogenic risk remains negligible across all sources, whereas carcinogenic risk is driven by upper-tail conditions but remains within the cautionary range. Traffic emissions consistently represent the dominant contributor to both HI and TCR, followed by service-industrial sources, while natural sources contribute mainly to baseline exposure. These findings highlight the importance of prioritizing traffic and service-industrial emissions in risk mitigation strategies for rapidly urbanizing coastal cities.

3.6. Comparison with industrial cities

URD in Da Nang shows much lower mean concentrations of most PTEs than those reported in industrial cities, especially in northern and

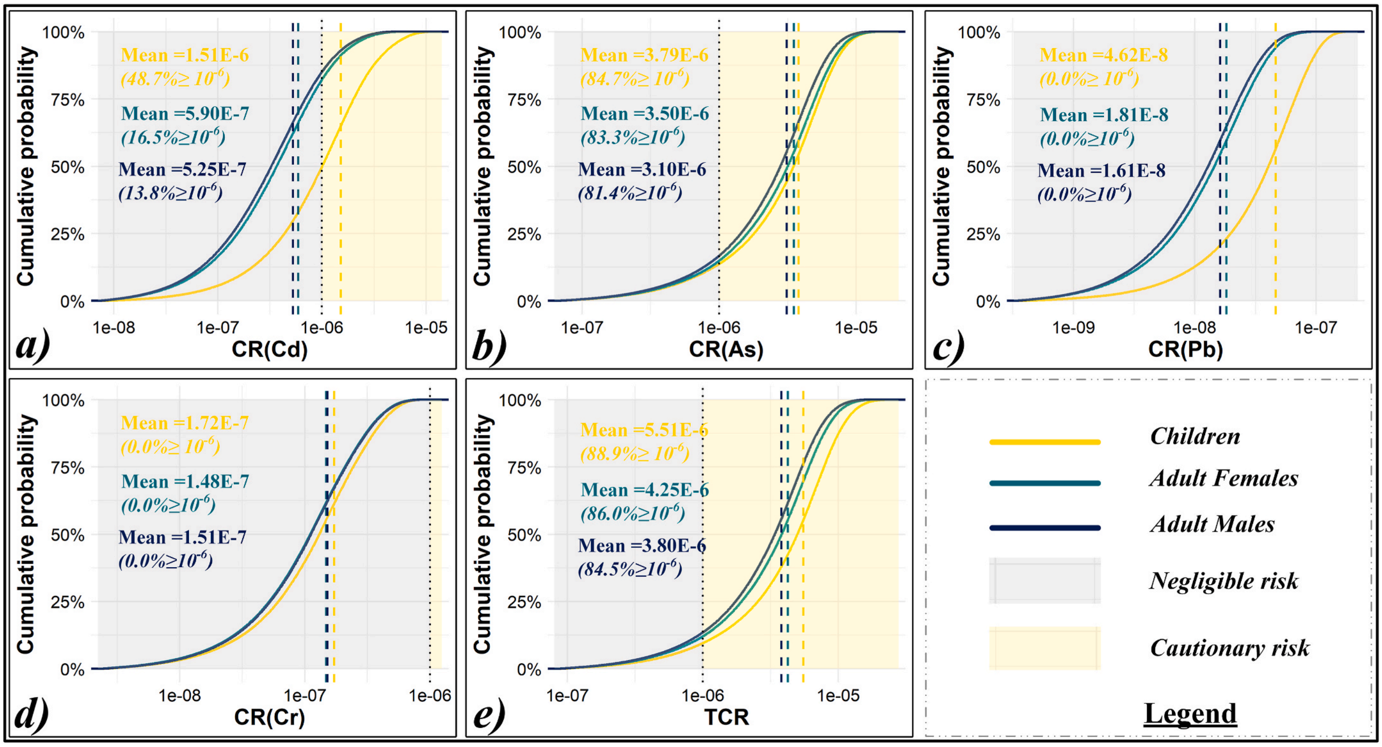

Fig. 5. ECDFs of carcinogenic risk: (a-d) CR for individual PTEs and (e) *TCR* for children, adult females, and adult males. Dashed lines indicate means; dotted line indicates the benchmark (1×10^{-6}).

central China, Africa, the Americas, and Europe (Table S5). For example, reported mean concentrations of key elements such as mean Cd (1.8-4.5 mg/kg), Pb (38-106 mg/kg), and Cr (89-296 mg/kg) in cities such as Datong, Xi'an, Jinan, and Shijiazhuang are consistently higher than in Da Nang (Wang et al., 2024; Wang et al., 2023b; Yang et al., 2024). This reflects ongoing industrial emissions and long-term accumulation.

Despite these differences in mean contamination, probabilistic comparisons indicate a consistent pattern in which pollution behavior is governed more by variability and risk structure than by average concentrations. In both industrial cities and Da Nang, a limited group of elements (notably Cd and Sb) dominates probabilistic pollution indicators, showing pronounced right-skewed distributions toward higher I_{geo} classes. The key distinction lies in spatial organization: industrial cities tend to exhibit more spatially consistent and elevated *INI* levels, whereas Da Nang is characterized by moderate mean *INI* but strong upper-tail behavior (P95), indicating localized hotspots influenced by monsoon-driven resuspension and heterogeneous land use (Arfaeinia et al., 2019; Osorio-Martinez et al., 2021).

Ecological risk patterns further reinforce these contrasts. Across different urban contexts, ecological risk is typically controlled by a small subset of elements, particularly Cd (and Cr in some cases), rather than uniformly distributed across all PTEs (Wang et al., 2024; Wang et al., 2023b; Yang et al., 2023a; Yang et al., 2024). In industrial cities, this often results in high mean NCRI values (>200), indicating considerable to high ecological risk. By contrast, Da Nang exhibits low mean NCRI but pronounced upper-tail risk levels, where “high” or “very high ecological risk” levels occur in localized areas associated with traffic and service-industrial sources enriched in Cd and Sb. Similar hotspot-driven risk patterns have been reported in coastal urban environments such as Bandar Abbas (Heidari et al., 2021).

Human health risks comparisons show similarly consistent patterns. In most industrial cities, non-cancer risk for children often meets or exceeds the benchmark ($HI = 1$), driven by key toxic elements such as Cr, Pb, and As (Öncü et al., 2025; Wang et al., 2024; Yang et al., 2023a; Yüksel et al., 2025). In Da Nang, *HI* is below the threshold for all groups, indicating lower overall non-carcinogenic risk. However, carcinogenic risk shows convergence across urban contexts, with *TCR* generally falling within the cautionary range (10^{-6}-10^{-4}), dominated by As (60-80%). Notably, the probability of *TCR* exceeding 10^{-6} for children in Da Nang is comparable to those in industrial cities, despite lower contamination (Yang et al., 2024; Yang et al., 2023b).

Source-resolved comparisons highlight systematic differences in risk drivers. In industrial cities, ecological and health risks are mainly associated with service-industrial emissions and coal combustion, whereas in Da Nang, traffic-related non-exhaust emissions play a dominant role in human health risk, and service-industrial activities control ecological risk hotspots. Overall, these comparisons indicate that lower mean concentrations do not necessarily translate into lower risk, as risk is governed by source-specific contributions and upper-tail behavior. This underscores the importance of source-oriented probabilistic frameworks for assessing environmental risks in rapidly urbanizing tropical coastal cities.

3.7. *Advantages of an open-source PMF-MCS framework*

This study uses a fully open-source PMF-MCS framework for SO-PRA, offering clear advantages over commercial platforms. Full R script documentation ensures transparent and reproducible analysis for distribution fitting, MCS, and risk estimation. This allows direct tracking of how uncertainty leads to shifts in ecological risk levels. PMF settings and diagnostics can be easily repeated or changed, making verification and comparison across locations straightforward. Results show that simulated and observed means (e.g., *NCRI*, *HI*, *TCR*) closely match, confirming the R-based method maintains accuracy.

The integration of PMF outputs with probabilistic modeling within a single environment reduces data-transfer errors and enables consistent evaluation of source-specific ecological and health risk. This flexible and cost-effective approach is particularly suitable for rapidly urbanizing regions with limited technical and financial resources.

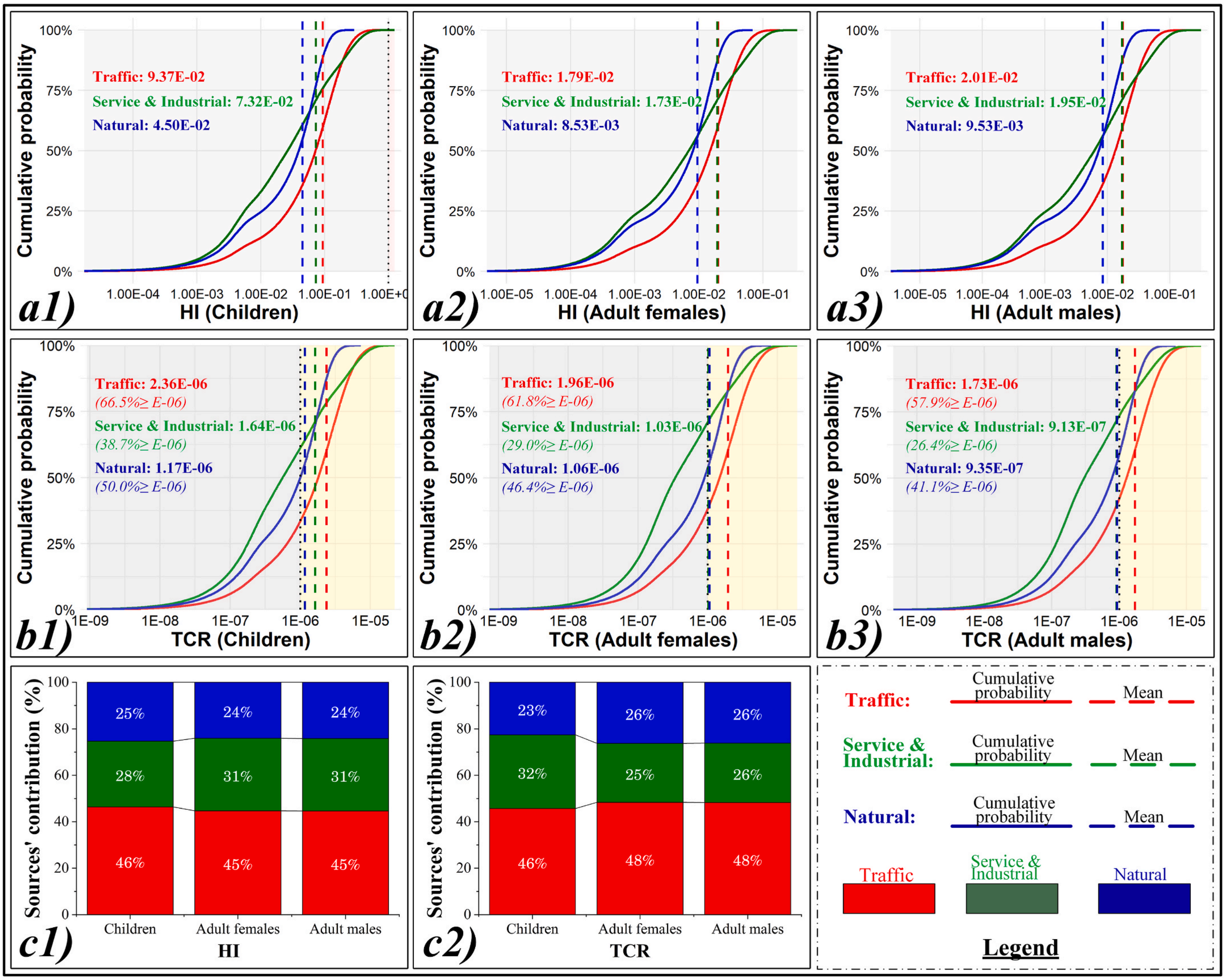

Fig. 6. Source-resolved cumulative probability distributions of *HI* (a1-a3) and *TCR* (b1-b3) for children, adult females, and adult males based on PMF-integrated MCS; (c1-c2) relative source contributions to *HI* and *TCR*.

3.8. Implications for urban environmental management

Source-oriented probabilistic assessment shows that environmental and health risks in Da Nang are systematically underestimated by deterministic approaches. Mean-based indices classify risk as “low”, but probabilistic percentiles reveal localized hotspot conditions reaching “high” to “very high” ecological risk levels, representing upper-tail probabilities rather than widespread city-scale risk. This contrast highlights the importance of probabilistic, source-based approaches for identifying and managing localized high-risk areas in tropical coastal cities. Traffic-related non-exhaust emissions dominate risk, contributing 49.8% of *NCRI* and 46-48% of *TCR*, even with only moderate mean concentrations. Mitigation should prioritize traffic-focused measures, such as low-emission brake and tire standards, traffic optimization, and enhanced street sweeping in busy corridors. Sb also emerges as a critical but under-monitored indicator: despite a low mean (1.62 mg/kg), it shows the strongest enrichment (28-fold over background) and drives 70.9-93.7% of *INI* variability, often causing localized conditions to shift from "heavily" to "extremely contaminated".

Population-specific vulnerability narrows management priorities. Non-carcinogenic risks (*HI*) remain below thresholds across all groups, while carcinogenic risks for children fall within the “cautionary range” (10^{-6}-10^{-4}), with a high probability (up to 88.9%) of cases exceeding the acceptable level ($TCR>10^{-6}$). These results suggest the need for targeted exposure reduction in environments frequently accessed by children. The sources that drive the greatest ecological and health risks are not necessarily those with the highest average concentrations. Instead, upper-tail risk is controlled by hotspots of Cd, Sb, and As. These findings indicate that risk in tropical coastal cities is governed more by spatial heterogeneity and upper-tail behavior than by mean contamination levels.

4. Conclusions

This study applied a fully SO-PRA framework to urban road dust in Da Nang, a rapidly urbanizing tropical coastal city in Southeast Asia. The research combines PMF-based source apportionment with MCS. It provides a region-specific demonstration showing how emission sources translate into ecological and human health risks under uncertainty.

Three dominant sources were identified based on PMF inference: traffic emissions (44.8%), service-industrial activities (30.1%), and natural background (25.2%). Mean indices show contamination as “uncontaminated to moderately contaminated” and ecological risk as “low ecological risk”. However, probabilistic analysis identifies localized hotspots where Cd and Sb may drive ecological risk into "high" and "very high" categories at upper percentiles, indicating low-probability, high-impact conditions rather than widespread risk across the city. In these hotspots, Cd and Sb trigger transitions to "high" and "very high ecological risk". Ecological risk is mainly controlled by service-industrial sources through Cd-dominated upper-tail *NCRI* behavior. Traffic-related non-exhaust emissions dominate both non-carcinogenic and carcinogenic health risks. Children are the most vulnerable group, and As is the primary contributor to carcinogenic risk, with TCR values generally within the cautionary range (10^{-6}-10^{-4}), particularly for children, but remaining below the unacceptable threshold.

Overall, these findings show that lower mean contamination may still be associated with elevated risks under upper-tail conditions, reflecting localized hotspot-driven rather than widespread risk. The proposed open-source PMF-MCS framework provides a transparent and reproducible approach for source-oriented probabilistic risk assessment, supporting targeted environmental management.

CRediT authorship contribution statement

Tra Van Tung: Writing – original draft, Visualization, Methodology, Formal analysis, Data curation, Conceptualization. **Tinh H.T. Nguyen:** Writing – original draft, Methodology, Investigation, Data curation, Conceptualization. **Tanapon Phenrat:** Writing – review & editing, Validation, Supervision, Conceptualization. **Tran Cong-Thanh:** Visualization, Software, Methodology, Formal analysis, Data curation, Conceptualization. **Ly Sy Phu Nguyen:** Methodology, Formal analysis, Data curation, Conceptualization. **Vinh Son Lam:** Validation, Supervision, Methodology. **Bui Pham Phuong Thanh:** Writing – original draft, Validation, Methodology, Conceptualization. **Nguyen Xuan Cuong:** Visualization, Software, Methodology, Investigation, Formal analysis, Data curation, Conceptualization. **Quoc Ba Tran:** Writing – review & editing, Visualization, Software, Methodology, Investigation, Formal analysis, Data curation, Conceptualization.

Funding

This research is funded by the National Foundation for Science and Technology Development, Vietnam (NAFOSTED) under grant number 105.99-2020.15.

Declaration of competing interest

The authors declare that they have no known competing financial interests or personal relationships that could have appeared to influence the work reported in this paper.

Acknowledgment

The authors gratefully acknowledge the lecturers and students from the Faculty of Environmental and Chemical Engineering, Duy Tan University, for their assistance in road dust sample collection. The Center for Development of Community Initiative and Environment is acknowledged for its support in sample collection and processing. The authors also acknowledge support from the Frontier Research and Innovation Cluster Fund, Naresuan University (Grant No. R2569C005).

Appendix A. Supplementary data

Supplementary data to this article can be found online at https://doi.org/10.1016/j.envpol.2026.128234.

Data availability

Data will be made available on request.

References

Adewumi, A.J., 2022. Heavy metals in soils and road dust in akure City, Southwest Nigeria: pollution, sources, and ecological and health risks. Expo. Health 14, 375–392. https://doi.org/10.1007/s12403-021-00456-y.

Akindele, S.O., Oguntoke, O., Badejo, A.A., Taiwo, A.M., 2024. Pollution and health risks of potentially toxic elements in road dust from Ibadan, Nigeria. Chem. Afr. 7, 4393–4410. https://doi.org/10.1007/s42250-024-01075-1.

Albuja, M., Jeong, H., Ra, K., 2024. Distribution of potentially toxic elements and health risk assessment of road dust in a steel industrial area. Int. J. Environ. Sci. Technol. 21, 4967–4978. https://doi.org/10.1007/s13762-023-05327-4.

Arfaeinia, H., Dobaradaran, S., Moradi, M., Pasalari, H., Mehrizi, E.A., Taghizadeh, F., Esmaili, A., Ansarizadeh, M., 2019. The effect of land use configurations on concentration, spatial distribution, and ecological risk of heavy metals in coastal sediments of northern part along the Persian Gulf. Sci. Total Environ. 653, 783–791. https://doi.org/10.1016/j.scitotenv.2018.11.009.

Asgari, A., Sobhanardakani, S., Cheraghi, M., Lorestani, B., Sadr, M.K., 2025. Source apportionment, ecological and health risks of potentially toxic elements in street dusts across different land uses in city of Kermanshah, Iran. Sci. Rep. 15, 2517. https://doi.org/10.1038/s41598-025-86677-6.

Cao, Y., Li, X., He, F., Sun, X., Zhang, X., Yang, T., Dong, J., Gao, Y., Zhou, Q., Shi, D., Wang, J., Yu, H., 2021. Comprehensive screen the lead and other toxic metals in total environment from a coal-gas industrial city (NW, China): based on integrated source-specific risks and site-specific blood lead levels of 0–6 aged children. Chemosphere 278, 130416. https://doi.org/10.1016/j.chemosphere.2021.130416.

Chen, L., Fang, L., Yang, X., Luo, X., Qiu, T., Zeng, Y., Huang, F., Dong, F., White, J.C., Bolan, N., Rinklebe, J., 2024. Sources and human health risks associated with potentially toxic elements (PTEs) in urban dust: a global perspective. Environ. Int. 187, 108708. https://doi.org/10.1016/j.envint.2024.108708.

Dobaradaran, S., Nabipour, I., Saeedi, R., Ostovar, A., Khorsand, M., Khajeahmadi, N., Hayati, R., Keshtkar, M., 2017. Association of metals (Cd, Fe, As, Ni, Cu, Zn and Mn) with cigarette butts in northern part of the Persian Gulf. Tob. Control 26, 461–463. https://doi.org/10.1136/tobaccocontrol-2016-052931.

Dytłow, S., Górka-Kostrubiec, B., 2021. Concentration of heavy metals in street dust: an implication of using different geochemical background data in estimating the level of heavy metal pollution. Environ. Geochem. Health 43, 521–535. https://doi.org/10.1007/s10653-020-00726-9.

Gunawardana, C., Goonetilleke, A., Egodawatta, P., Dawes, L., Kokot, S., 2012. Source characterisation of road dust based on chemical and mineralogical composition. Chemosphere 87, 163–170. https://doi.org/10.1016/j.chemosphere.2011.12.012.

Hakanson, L., 1980. An ecological risk index for aquatic pollution control. A sedimentological approach. Water Res. 14, 975–1001. https://doi.org/10.1016/0043-1354(80)90143-8.

Hao, Q., Lu, X., Yu, B., Yang, Y., Lei, K., Pan, H., Gao, Y., Liu, P., Wang, Z., 2023. Sources and probabilistic ecological-health risks of heavy metals in road dust from urban areas in a typical industrial city. Urban Clim. 52, 101730. https://doi.org/10.1016/j.uclim.2023.101730.

Heidari, M., Darijani, T., Alipour, V., 2021. Heavy metal pollution of road dust in a city and its highly polluted suburb; quantitative source apportionment and source-specific ecological and health risk assessment. Chemosphere 273, 129656. https://doi.org/10.1016/j.chemosphere.2021.129656.

Huang, J., Wu, Y., Sun, J., Li, X., Geng, X., Zhao, M., Sun, T., Fan, Z., 2021. Health risk assessment of heavy metal(loid)s in park soils of the largest megacity in China by using Monte Carlo simulation coupled with positive matrix factorization model. J. Hazard. Mater. 415, 125629. https://doi.org/10.1016/j.jhazmat.2021.125629.

Jeong, H., Ra, K., 2022. Source apportionment and health risk assessment for potentially toxic elements in size-fractionated road dust in Busan Metropolitan City, Korea. Environ. Monit. Assess. 194, 350. https://doi.org/10.1007/s10661-022-10008-9.

Khan, R., Basir, M.S., Anik, A.H., Akhi, S.Z., Khan, M.H.R., Sultana, S., Aldawood, S., Parvez, M.S., Idris, A.M., Roy, D.K., 2025. Sources and distribution of potentially toxic elements in urban road dust: a comparative insights and risk assessment of two polluted cities. Environ. Pollut. 368, 125768. https://doi.org/10.1016/j.envpol.2025.125768.

Krupnova, T.G., Rakova, O.V., Gavrilkina, S.V., Antoshkina, E.G., Baranov, E.O., Yakimova, O.N., 2020. Road dust trace elements contamination, sources, dispersed composition, and human health risk in Chelyabinsk, Russia. Chemosphere 261, 127799. https://doi.org/10.1016/j.chemosphere.2020.127799.

Kurmus, H., Mohajerani, A., 2020. Leachate analysis of heavy metals in cigarette butts and bricks incorporated with cigarette butts. Materials 13, 28–43. https://doi.org/10.3390/ma13122843.

Liu, L., Liu, Q., Ma, J., Wu, H., Qu, Y., Gong, Y., Yang, S., An, Y., Zhou, Y., 2020. Heavy metal(loid)s in the topsoil of urban parks in Beijing, China: concentrations, potential sources, and risk assessment. Environ. Pollut. 260, 114083. https://doi.org/10.1016/j.envpol.2020.114083.

Luo, H., Wang, Q., Guan, Q., Ma, Y., Ni, F., Yang, E., Zhang, J., 2022. Heavy metal pollution levels, source apportionment and risk assessment in dust storms in key cities in Northwest China. J. Hazard. Mater. 422, 126878. https://doi.org/10.1016/j.jhazmat.2021.126878.

Luo, X., Ren, B., Hursthouse, A.S., Thacker, J.R.M., Wang, Z., 2020. Soil from an abandoned manganese mining area (Hunan, China): significance of health risk from potentially toxic element pollution and its spatial context. Int. J. Environ. Res. Publ. Health 17. https://doi.org/10.3390/ijerph17186554.

Mielke, H.W., Laidlaw, M.A.S., Gonzales, C.R., 2011. Estimation of leaded (Pb) gasoline's continuing material and health impacts on 90 US urbanized areas. Environ. Int. 37, 248–257. https://doi.org/10.1016/j.envint.2010.08.006.

Müller, G., 1969. Index of geo accumulation in sediments of the Rhine River. Geology Journal 2 (3), 108–118.

Navrotsky, A., 1994. Physics and Chemistry of Earth Materials. Cambridge University Press.

NIST, 2020. SRM 1648a - Urban Particulate Matter. Certificate of Analysis of National Institute of Standards & Technology, Gaithersburg, MD, USA.

Öncü, T., Yazman, M.M., Ustaoğlu, F., Hristova, E., Yüksel, B., 2025. Source dynamics and environmental risk of street dust as a vector of human exposure to potentially toxic elements in Istanbul, Türkiye. Sci. Rep. 15, 30550. https://doi.org/10.1038/s41598-025-11472-2.

Osorio-Martinez, J., Silva, L.F., Flores, E.M., Nascimento, M.S., Picoloto, R.S., Olivero-Verbel, J., 2021. Environmental and Human Health Risks Associated with Exposure to Hazardous Elements Present in Urban Dust from Barranquilla, Colombian Caribbean. Wiley Online Library.

Panqing, Y., Abliz, A., Xiaoli, S., Aisaiduli, H., 2023. Human health-risk assessment of heavy metal–contaminated soil based on Monte Carlo simulation. Sci. Rep. 13, 7033. https://doi.org/10.1038/s41598-023-33986-3.

Rehman, A., Zhong, S., Du, D., Zheng, X., Ijaz, S., Haider, M.I.S., Hussain, M., 2025. Unveiling sources, contamination, and eco-human health implications of potentially toxic metals from urban road dust. Sci. Rep. 15, 10673. https://doi.org/10.1038/s41598-025-95205-5.

Tran, Q.B., Nguyen, L.S.P., Cuong, N.X., Nguyen, T.H.T., Vu, T.X., Hau, L.Q., Dat, N.D., 2025. Assessment of road dust heavy metal pollution and health risk in urban-industrial transition zones: implications on environmental management for emerging cities. Int. J. Environ. Res. 19, 185. https://doi.org/10.1007/s41742-025-00848-x.

Tran, V.V., 2025. Statistical Yearbook of Danang 2024. Statistical Publishing House, Danang, Vietnam.

US.EPA, 2009. Risk Assessment Guidance for Superfund Volume I: Human Health Evaluation Manual (Part F, Supplemental Guidance for Inhalation Risk Assessment). Environmental Protection Agency, Washington, D.C., p. 68

US.EPA, 2014. EPA Positive Matrix Factorization (PMF) 5.0 Fundamentals and User Guide. US Environmental Protection Agency, Washington, DC, p. 136.

Ustaoğlu, F., Yazman, M.M., Batan, N., Yüksel, B., 2026. Disaster-induced toxic metal mobilization in post-earthquake street dust of Adıyaman, Türkiye: pollution indices, receptor model source apportionment, and probabilistic health risk evaluation. J. Hazard Mater. 506, 141606. https://doi.org/10.1016/j.jhazmat.2026.141606.

Wang, N., Wang, A., Kong, L., He, M., 2018. Calculation and application of Sb toxicity coefficient for potential ecological risk assessment. Sci. Total Environ. 610–611, 167–174. https://doi.org/10.1016/j.scitotenv.2017.07.268.

Wang, X., Gao, Q., Wang, W., Yan, J., Liu, Y., Kuang, S., Lu, J., 2024. Determining priority control factors for heavy metal management in urban road dust based on source-oriented probabilistic ecological-health risk assessment: a study in Xi'an during peak pollution season. J. Environ. Manag. 369, 122105. https://doi.org/10.1016/j.jenvman.2024.122105.

Wang, X., Liu, E., Yan, M., Zheng, S., Fan, Y., Sun, Y., Li, Z., Xu, J., 2023a. Contamination and source apportionment of metals in urban road dust (Jinan, China) integrating the enrichment factor, receptor models (FA-NNC and PMF), local Moran's index, Pb isotopes and source-oriented health risk. Sci. Total Environ. 878, 163211. https://doi.org/10.1016/j.scitotenv.2023.163211.

Wang, Z., Lu, X., Yang, Y., Yu, B., Lei, K., Pan, H., Fan, P., Zuo, L., 2023b. Estimation of probabilistic environmental risk of heavy Metal(loid)s in resuspended megacity street dust with Monte Carlo simulation. Minerals 13. https://doi.org/10.3390/min13030305.

Wu, Y., Xia, Y., Mu, L., Liu, W., Wang, Q., Su, T., Yang, Q., Milinga, A., Zhang, Y., 2024. Health risk assessment of heavy metals in agricultural soils based on multi-receptor modeling combined with Monte Carlo simulation. Toxics 12. https://doi.org/10.3390/toxics12090643.

Yang, Y., Lu, X., Fan, P., Yu, B., Wang, L., Lei, K., Zuo, L., 2023a. Multi-element features and trace metal sources of road sediment from a mega heavy industrial city in North China. Chemosphere 311, 137093. https://doi.org/10.1016/j.chemosphere.2022.137093.

Yang, Y., Lu, X., Yu, B., Wang, Z., Wang, L., Lei, K., Zuo, L., Fan, P., Liang, T., 2024. Exploring the environmental risks and seasonal variations of potentially toxic elements (PTEs) in fine road dust in resource-based cities based on Monte Carlo simulation, geo-detector and random forest model. J. Hazard. Mater. 473, 134708. https://doi.org/10.1016/j.jhazmat.2024.134708.

Yang, Y., Lu, X., Yu, B., Zuo, L., Wang, L., Lei, K., Fan, P., Liang, T., Rennert, T., Rinklebe, J., 2023b. Source-specific risk judgement and environmental impact of potentially toxic elements in fine road dust from an integrated industrial city, North China. J. Hazard. Mater. 458, 131982. https://doi.org/10.1016/j.jhazmat.2023.131982.

Yuksel, B., Kaya-Akyuzlu, D., Kayaalti, Z., Ozdemir, F., Soylemez-Gokyer, D., Soylemezoglu, T., 2017. Study of blood iron vs. blood lead levels in beta-thalassemia patients in Turkey: an application of analytical toxicology. https://doi.org/10.46770/AS.2010.01.001.

Yüksel, B., Mergen, G., Söylemezoglu, T., 2010. Assessment of arsenic levels in human hair by hydride generation atomic absorption spectrometry: a toxicological application. At. Spectrosc. 31, 1. https://doi.org/10.46770/AS.2017.02.006.

Yüksel, B., Öncü, T., Yazman, M.M., Hristova, E., Ustaoglu, F., 2025. P30-07 assessment of potentially toxic elements in urban street dust of istanbul: spatial distribution, source apportionment, and health risk implications. Toxicol. Lett. 411, S377. https://doi.org/10.1016/j.toxlet.2025.07.870.

Zafra-Mejía, C.A., Rondón-Quintana, H.A., 2025. Analysis of the potential availability of resuspended heavy metals from urban road sediments: a post-runoff approach. Environ. Pollut. 387, 127322. https://doi.org/10.1016/j.envpol.2025.127322.

Zupančič, M., Miler, M., Žibret, G., 2024. The relationship between the inhalation bioaccessibility of potentially toxic elements in road dust from a heavily polluted industrial area and the source of their pollution. Environ. Pollut. 361, 124810. https://doi.org/10.1016/j.envpol.2024.124810.